Fiber optic extensometer for concrete deformation measurements

Libo Yuan, Li-min Zhou, K. T. Lau, Wei Jin, and M. S. Demokan

Citation: Rev. Sci. Instrum. **73**, 2469 (2002); doi: 10.1063/1.1445862
View online: http://dx.doi.org/10.1063/1.1445862
View Table of Contents: http://rsi.aip.org/resource/1/RSINAK/v73/i6
Published by the American Institute of Physics.

Fiber optic extensometer for concrete deformation measurements

Libo Yuan[a)]
Department of Physics, Harbin Engineering University, Harbin 150001, People's Republic of China and Department of Mechanical Engineering, The Hong Kong Polytechnic University, Hong Kong

Li-min Zhou and K. T. Lau
Department of Mechanical Engineering, The Hong Kong Polytechnic University, Hong Kong

Wei Jin and M. S. Demokan
Department of Electrical Engineering, The Hong Kong Polytechnic University, Hong Kong

(Received 6 June 2001; accepted for publication 3 December 2001)

A fiber optic extensometer based on a scanning white light Michelson interferometer is presented. The instrument employs a light emitting diode as the light source and a single mode fiber with predetermined gauge length as the extensometer sensor head. Light to and from the sensor head is transmitted through a single mode lead (i.e., in/out) fiber. The sensor performance is insensitive to the in/out fiber extensions. The fiber optic extensometer was applied to measure the compression and tension of concrete specimens. The measurement results compare well with that from a conventional extensometer. © *2002 American Institute of Physics.* [DOI: 10.1063/1.1445862]

I. INTRODUCTION

Fiber optic sensors have been widely studied because of their well-known advantages such as immunity to electromagnetic interference, ability to operate in hostile environment, high sensitivity, and potential for multiplexing.[1] The small dimension and high mechanical strength of the glass optical fibers also enable them to be used as embedded sensors for concrete[2] or other composite materials.[3]

This article reports an optical fiber extensometer instrument for the measurement of concrete deformation. The extensometer is based on a scanning white light Michelson interferometer. The basic principle of the technique will be presented in Sec. II; an analysis on the signal intensity is given in Sec. III. Strain transfer from concrete to fiber is discussed in Sec. IV, and test results on concrete specimens with surface mounted and embedded sensors are presented in Sec. V.

II. MEASUREMENT PRINCIPLE

Figure 1 shows the instrument configuration of the extensometer. The system is basically a modified fiber optic Michelson interferometer with a sensing arm and a reference arm connected to the two ports of a 2×2 directional coupler. The sensing arm consists of a lead in/out fiber and a sensing fiber region defined between the two reflectors as shown in Fig. 1. The reference arm consists of a fiber coupler loop, a collimator lens, and a scanning reflecting mirror. The coupler loop generates reference signals of multiple optical paths that are used to match the signals from two reflectors. The Michaelson interferometer is powered by a broadband light emitting diode (LED), and the output signal from the interferometer is detected using a PIN photodetector connected to a personal computer for further signal processing. Interferometric signals are generated when the scanning mirror is at positions where the optical path length of a reference signal is matched to a signal reflected from one of the reflectors. The difference in the positions of the scanning mirror is then equal to the sensing gauge length that is sensitive to deformation or strain applied to the sensing fiber.

The detailed principle can be explained by using the diagrams shown in Fig. 2. Light from the LED is split into two beams of approximately equal intensity by the coupler, one into the sensing arm and the other the reference arm. Light in the sensing arm propagates along the lead fiber of length L_1 and then further into the sensing region of length L_0. During propagation, two reflected signals are generated. One from the joint between the lead and the sensing fiber (reflected signal 1), the other from the far end of the sensing fiber (reflected signal 2). The two reflected signals return to the photodetector (PD) through the same lead fiber and the directional coupler. The optical paths experienced by the two reflected signals are, respectively, $2L_1n$ and $2L_1n+2L_0n$, where n is the effective refractive index of the guided mode in the optical fiber.

Light in the reference arm is guided through a fiber coupler loop, a graded index (GRIN) collimator lens, to a mirror mounted on a scanning translation stage where light is reflected. The reflected light returned, through the same fiber path, to the photodetector. The length of the reference arm excluding the coupler loop is L_2 while the couple loop length is L. The use of the coupler loop generates multiple reference beams with corresponding path length

$$2L_2n+iLn+2X, \tag{1}$$

where $i=0,1,2,...$ is the number of light circulation through the coupler loop. X is the gap distance between the GRIN lens and the mirror. If L_2 and L are chosen, respectively, to be approximately equal but slightly shorter than L_1 and L_0, the optical path lengths of the reference signals can then be

[a)]Electronic mail: lbyuan@vip.sina.com

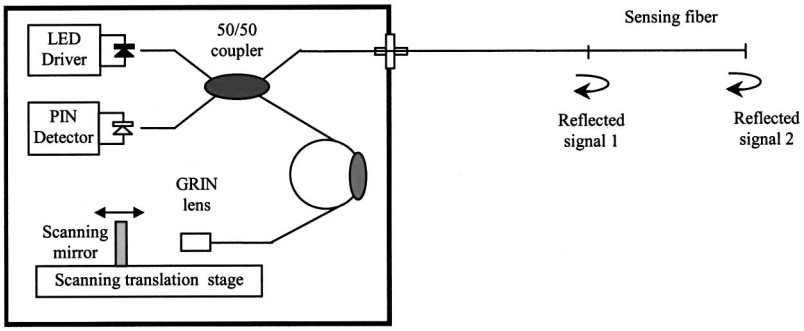

FIG. 1. Instrument configuration of the fiber optic extensometer.

matched to that of the reflected signals from the sensing arm by slightly adjusting the mirror position (i.e., the value of X). White light interferometric patterns are then generated around the matching positions. The first interferometric pattern, corresponds to the path length match of the first reflected signal from the sensing arm to that of the first reference signal, i.e., $i=0$ in Eq. (1). The central fringe, which is located in the center of the fringe pattern and has the highest amplitude, corresponds to the exact optical path matching and is given by

$$2L_1n=2L_2n+2X_1. \tag{2}$$

Similarly, the second interferometric pattern is generated when the mirror is tuned to a position $X=X_2$ where the optical path length of the reflected signals from the far end is matched to that of the reference beam that travels through the reference fiber L_2 and the coupler loop length L twice. The exact path length matching is given by

$$2L_1n+2L_0n=2L_2n+2Ln+2X_2. \tag{3}$$

Using Eqs. (1) and (2), we obtain

$$nL_0-nL=(X_2-X_1)=\Delta X. \tag{4}$$

Here, $\Delta X=(X_2-X_1)$ is the difference between the two mirror positions corresponding to the two path-length matches. It can be seen that ΔX is independent of lead fiber, this is because the two reflected signals from the two ends of the gauge travels through the same lead in/out fiber, and the differential measurement removes the effect of the lead fiber and thus the effect of environmental variation on the lead fiber. This fact is important because the lead fiber can be made arbitrarily long for remote interrogation without introducing any degradation to the system performance. Because the optical path length of the coupler loop L can be preserved as constant by isolating it from strain and temperature, any variation in optical path length of the sensing fiber (nL_0) can then be deduced from the measured value of ΔX. If fiber gauge length L_0 is made approximately equal to that of the coupler loop length L, the scanning distance between the two

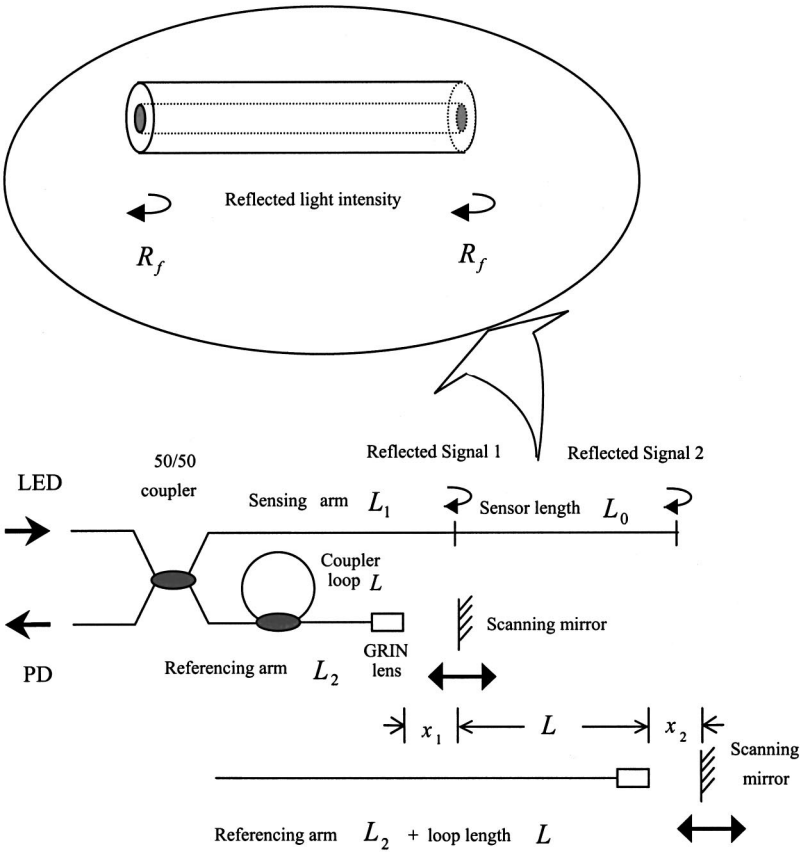

FIG. 2. Measurement principle of the fiber optic extensometer.

white light interference patterns $|X_2-X_1|$ can be made very short. This avoids the use of a long-range translation stage and thus results in a lower cost system. The short scanning distance also allows a faster system to be built, compared with the conventional white light systems where a large scanning range is usually required. The gauge may be designed to have an arbitrarily long length, as long as a similar length of fiber is used to form the couple loop, without the need to increase the scanning range.

If the sensing fiber is embedded within a concrete structure, as the structure deforms, the optical path of the sensing fiber will vary due to the physical length extension (or compression) and the change of refractive index of the fiber. The change in optical path length may be expressed as

$$\delta(\Delta X)=n\,\delta L_0+\delta n L_0. \tag{5}$$

The first term δL_0 in Eq. (5) represents the physical length change and is directly proportional to the axial strain ($\varepsilon_{\text{fiber}}$) applied to the sensing fiber through the expression

$$\delta L_0(\varepsilon_{\text{fiber}})=L_0\varepsilon_{\text{fiber}}. \tag{6}$$

The second term in Eq. (5) is the change in optical path due to a change in the refractive index of the fiber core, which is given by[4]

$$\delta n=-\tfrac{1}{2}n^3[(1-\mu)p_{12}-\mu p_{11}]\varepsilon_{\text{fiber}}, \tag{7}$$

where μ and p_{ij} are, respectively, the Poisson's ratio and the elements of the strain-optic tensor of the fiber material.

Substituting Eqs. (6) and (7) into Eq. (5), we obtain the optical path length variation of the sensing fiber as

$$\begin{aligned}\delta(\Delta X)&=nL_0\varepsilon_{\text{fiber}}-\tfrac{1}{2}n^3[(1-\mu)p_{12}-\mu p_{11}]L_0\varepsilon\\&=n_{\text{eff}}L_0\varepsilon_{\text{fiber}}\\&=n_{\text{eff}}\Delta L_0\end{aligned} \tag{8}$$

with

$$n_{\text{eff}}=\{n-\tfrac{1}{2}n^3[(1-\mu)p_{12}-\mu p_{11}]\}. \tag{9}$$

For the silica materials at wavelength $\lambda=1300$ nm, $n=1.46$, $\mu=0.25$, $p_{11}\approx 0.12$, $p_{12}\approx 0.27$,[5] giving $n_{\text{eff}}\approx 1.19$.

III. SIGNAL INTENSITY ANALYSIS

It has been shown in Sec. II that the extensometer is based on the measurement of the positions of the scanning mirror corresponding to the peaks of the white light interferometric fringe patterns. The peak intensities of the fringe patterns depend on the strength of the signals reflected from the sensing and the reference arms. In this section, we present the relation between peak intensities of the fringe patterns and the system parameters.

A. Reflected signals from the sensing arm

Assume that the light intensity from the LED source coupled into the optical fiber is I_0, and the couplers used are 50/50 couplers. Then the light intensity coupled into the sensing arm is $I_0\alpha/2$. Here α represents the insertion loss of the coupler and is defined as $\alpha=10^{(\delta/10)}$, where δ is the insertion loss of the coupler in dB. The intensities of the reflected light signals at the PD may be expressed as

$$\begin{cases}I_D(1)=I_0\alpha^2R_f/4\\ I_D(2)=I_0\alpha^2(1-R_f)^2R_f/4,\end{cases} \tag{10}$$

where $I_D(1)$ and $I_D(2)$ represent, respectively, the reflected light intensities from the end of the sensing fiber that joints with the lead fiber and from the far end of the sensing fiber. The reflectivity of the two ends are assumed, for simplicity, to be the same and equal to R_f. Under the condition of perpendicular incidence for the polished fiber end surface, the reflectivity is given by

$$R_f=\left(\frac{n-1}{n+1}\right)^2. \tag{11}$$

In fact, the received light intensities are less than that given in Eq. (10) due to the loss of the connection parts. The typical fiber connection loss was estimated to be 0.3 dB.

B. Reflected signals from the referencing arm

The reference light signal intensity corresponding to the path matching condition given by Eq. (2) may be expressed as

$$I'_D(1)=I_0\alpha^4\eta(X_1)R_m/16, \tag{12}$$

where R_m is the reflectivity of the mirror and $\eta(X)$ represents the light losses due to the GRIN lens collimator-mirror system, which may be expressed as[6]

$$\eta(X)=\frac{A}{[1+\xi X^{3/2}]^2}, \tag{13}$$

where A and ξ are dimensionless constants.

The intensity of the second reference signal corresponding to the path length matching condition given by Eq. (3) can be expressed as

$$I'_{D1}(2)=3I_0\alpha^6\eta(X_2)R_m/64. \tag{14}$$

C. Peak intensities of the fringe patterns

The first fringe pattern is due to the coherent mixing between the reflected signals from the sensing and the reference arms that satisfies Eq. (2). The peak intensity of this fringe pattern is

$$2\sqrt{I_D(1)I'_D(1)}=\frac{I_0\alpha^3}{4}\sqrt{\eta(X_1)R_fR_m}. \tag{15}$$

The second fringe pattern is due to the coherent mixing between the reflected signals from the sensing and the reference arms that satisfies Eq. (3). The peak intensity of this fringe pattern is

$$2\sqrt{I_D(2)I'_D(2)}=\frac{I_0\alpha^4}{8}\sqrt{3\,\eta(X_2)R_fR_m}. \tag{16}$$

To perform the fringe identification, the peak intensities of both fringe patterns should be made well above the system noise floor.

IV. STRAIN TRANSFER FROM CONCRETE TO FIBER

As has been discussed in Sec. III, the strain or deformation of the optical fiber embedded in the concrete materials can be related to the mirror displacement $\delta(\Delta X)$ by Eq. (8) and can then be measured. However, the strain or deformation experienced by the optical fiber may not be the same as that of the concrete (matrix) material, depending on the bonding characteristics between the matrix material and the optical fiber. If the matrix–glass fiber bond were perfect, then the strain that the glass fiber experienced would be equal to the strain in the surrounding matrix. However, in practice, the fiber has a polymer protective coating, and is far less rigid than the glass fiber and the concrete. Therefore, even with a perfect matrix–fiber bond, the layered cross section is expected to affect the performance of the fiber optic extensometer. It is obvious that the strain experienced by the optical fiber should always be less than the real strain within the concrete.

The concrete deformation can be related to fiber deformation by

$$\Delta L_{\text{concrete}} = \frac{\Delta L_0}{\kappa} \tag{17}$$

or expressed in terms of strain

$$\varepsilon_{\text{concrete}} = \frac{\varepsilon_{\text{fiber}}}{\kappa}. \tag{18}$$

Here, κ is a constant depending on the bonding characteristics between the fiber and host concrete. Calibration is generally performed to determine the value of κ for different bonding conditions. It will be shown in the next section that value of κ will be around 0.758 for the case where fiber is bonded on the surface of the specimen using epoxy, and 0.556 for fiber embedded within concrete specimen.

V. EXPERIMENTS AND RESULTS

Experiments were conducted using the setup shown in Fig. 1. The light source used was a commercial LED with a center wavelength of 1300 nm and a spectral width of about 30 nm. The mirror in the reference arm was mounted on a high-resolution positioning system with step resolution of 0.5 μm, and the accuracy and repeatability in identifying the central fringe of the white light interferometric pattern was estimated as less than $\pm$ one fringe, equivalent to 0.65 μm for the 1300 nm source.[7] The whole system is computerized and can perform automated and repeated measurement of optical path-length variation.

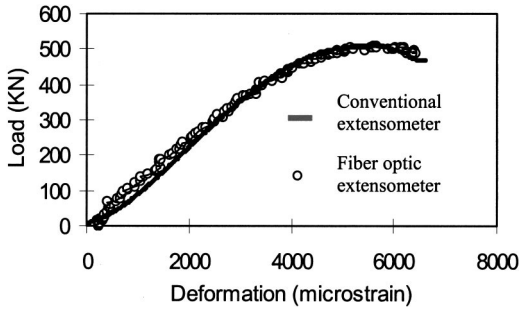

FIG. 4. Results of compression test.

A number of specimens were prepared with sensing fibers, either embedded within the structure during fabrication of the concrete or attached to the surface of the specimen after by way of adherents. Specimen mix proportions by weight of the concrete were 1:0.5:1.767:1.593 cement: water: sand: aggregate. Type No. 600 or No. 400 cement and maximum coarse aggregate size passing 9.5 mm and retained on a No. 4 sieve were used. Specimens were cast in 100 $\times$100$\times$300 (mm) steel moulds. The specimens were cured in a curing room for about four weeks before testing. The specimens made are of three types. The first specimen was designed for a compression test with 105.6 mm sensing fiber attached to the cleaned surface of the concrete specimen by epoxy as shown in Fig. 3. A conventional extensometer was set along side with the sensing fiber for comparison and calibration (Fig. 4). The second specimen was designed for a splitting tension test and again with a surface mounted sensing fiber of 103.8 mm (Figs. 5 and 6). The third type was designed for a compression test with an embedded fiber sensor as illustrated in Fig. 7. For this type, four specimens were prepared, the first two (No. 1 and No. 2 specimens) were made with No. 400 cement and the other two (No. 3 and No. 4) were with No. 600 cement. The fiber gauge lengths embedded within the four specimens were, respectively, 104.32, 102.51, 103.64, and 106.12 mm. When preparing the specimens with embedded sensors, the sensing fiber with polymer protective coating was first mounted at the center of steel

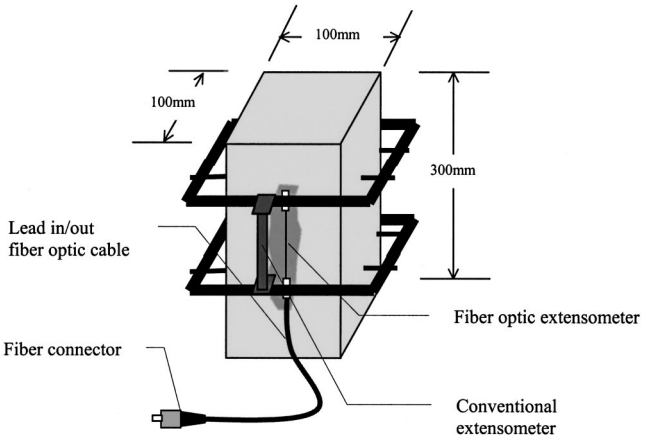

FIG. 3. Concrete specimen for compression test with surface mounted fiber gauge.

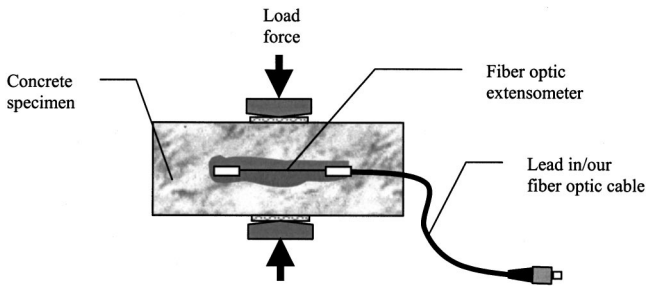

FIG. 5. Concrete specimen for splitting tension test with surface mounted fiber gauge.

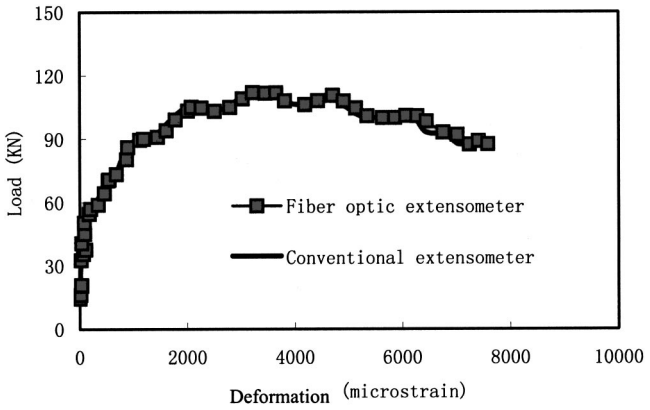

FIG. 6. Results of splitting tension test.

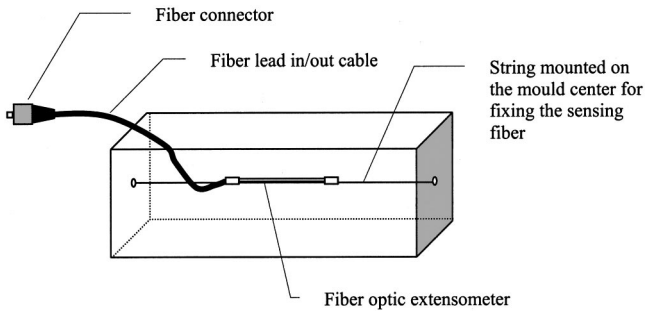

FIG. 7. Installation of the sensing fiber at the center of the concrete mould with the aid of a thin string.

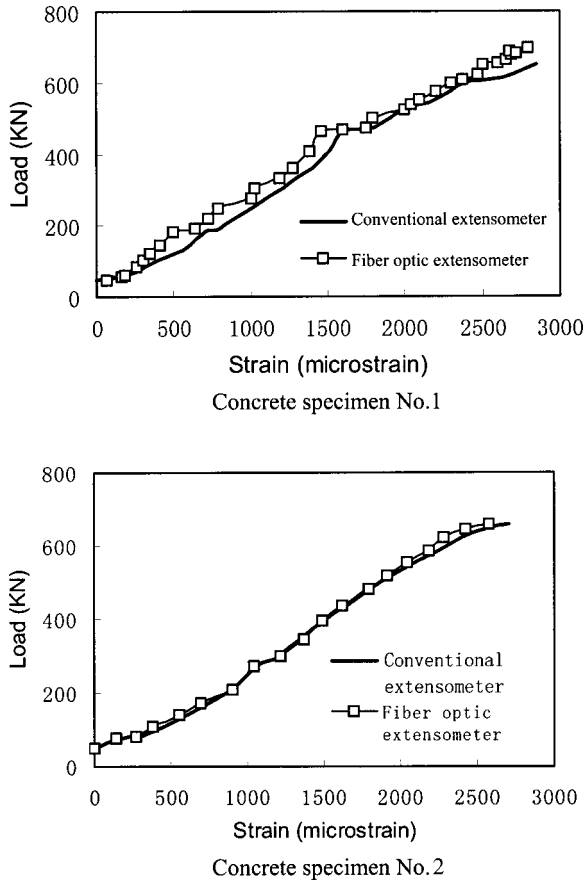

FIG. 8. Results of compression test with embedded fiber optic extensometer (lower strength concrete specimen with type No. 400 cement).

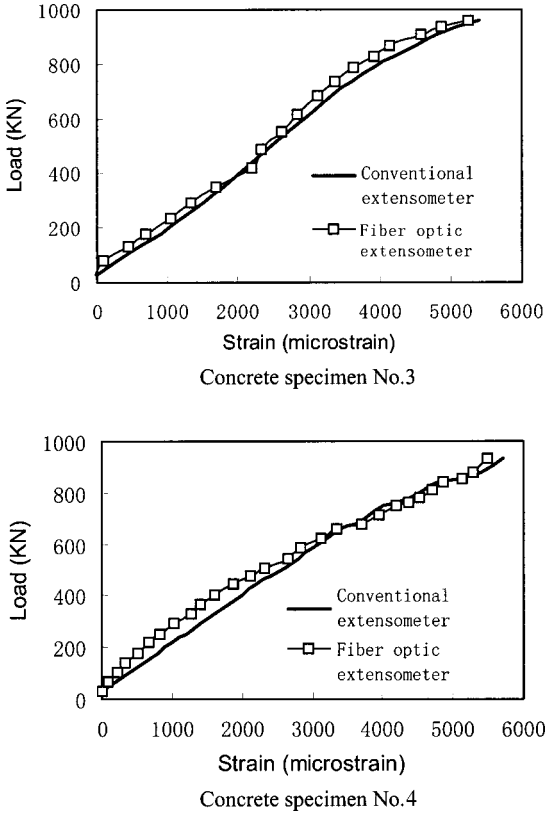

FIG. 9. Results of compression test with embedded fiber optic extensometer (higher strength concrete specimen with type No. 600 cement).

mould with the aid of a thin string which fixed at the center of mould shells (100×100 mm) as shown in Fig. 7. The concrete mixing material was then put into the mould. For each of the aforementioned specimens, a fiber connector was installed and polished at the ends of the extensometer pigtail fiber cable, in order to lead in the light source and lead out the reflective optical signals.

The results for compression and splitting tension tests are plotted, respectively, in Figs. 4 and 6. The measurement results from the conventional extensometer were fitted to that of the optical sensor by using a concrete to fiber strain transfer coefficient of $k=0.758$. The very close fits of both compression and splitting tension tests by the same strain transfer coefficient suggest that the coefficients for the surface mounted sensors are 0.758. For a compression test, the epoxy glued fiber optic extensometer debonded from the specimen surface when the deformation of concrete was beyond 6000 microstrains. For the splitting tension test, debonding did not occur until the applied strain was over 8000 microstrains.

The test results for the specimens with embedded sensors are plotted in Figs. 8 and 9, respectively, for low strength specimen (using No. 400 cement) and higher strength specimen (No. 600 cement). The results from the conventional gauge are the average of readings from two extensometers mounted in parallel to the embedded fiber on opposite sides of the specimens. These results were scaled to fit the fiber sensors readings by using a strain transfer coefficient 0.556. The results were fitted very well with the same

strain transfer coefficient for all four specimens, suggesting that the transfer coefficient for the embedded sensors was 0.556.

It should be noted that, for practical constructing concrete structures, a useful preembedded concrete bar sensor technique has been developed for the fiber optic extensometer.[8] The extensometer instrument can be used to measure tension, compression, to detect early cracks and to monitor the development of the micro cracks in civil structures.

ACKNOWLEDGMENTS

This work was supported by the National Natural Science Foundation of China, Grant No. 59879003, and the Science Foundation of Heilongjiang Province for Outstanding Youth, 1999, to Harbin Engineering University, and the research grant council of Hong Kong, PolyU5160/99E, and the Hong Kong Polytechnic University through Grant Nos. G-T096 and G-T282.

[1] E. Udd, Rev. Sci. Instrum. **66**, 4015 (1995).
[2] L. Yuan and F. Ansari, Meas. Sci. Technol. **9**, 261 (1998).
[3] R. O. Claus, K. D. Bennett, A. M. Vengsarkar, and K. A. Murphy, J. Nondestruct. Eval. **8**, 135 (1989).
[4] C. D. Butter and G. B. Hocker, Appl. Opt. **17**, 2867 (1978).
[5] D. A. Pinnow, in *Handbook of Lasers*, edited by R. J. Pressley (Chemical Rubber, Cleveland, OH, 1971).
[6] L. Yuan and L. Zhou, Appl. Opt. **37**, 4168 (1998).
[7] T. Li, A. Wang, K. Murphy, and R. Claus, Opt. Lett. **20**, 785 (1995).
[8] L. Yuan, W. Jin, L. Zhou and K. T. Lau, Sens. Actuators A **93**, 206 (2001).